Enhanced upwelling in the eastern equatorial Pacific at the last five glacial terminations

Hasrizal bin Shaari*, Masanobu Yamamoto and Tomohisa Irino

Faculty of Environmental Earth Science, Hokkaido University,
Kita-10, Nishi-5, Kita-ku, Sapporo 060-0810, Japan.

*Corresponding author: Tel.:+81-11-706-2379, fax:+81-11-706-4867
E-mail address: hasrizals@ees.hokudai.ac.jp (S.Hasrizal)

Keywords: TEX_{86}, U^{K}_{37}', eastern equatorial Pacific, upwelling, deglaciation

Abstract

TEX_{86}^{H}- and U^{K}_{37}'-derived paleotemperatures, and isoprenoid glycerol dialkyl glycerol tetraether (GDGT), and alkenone concentrations were examined for ODP Site 1239 in the eastern equatorial Pacific (EEP) for the last 430 kyrs. We propose that the difference between TEX_{86}^{H}- and U^{K}_{37}'-derived temperatures (ΔT) and the abundance ratio of GDGTs to alkenones (GDGT/alkenone ratio) are potential upwelling indices which show a consistent results with other upwelling indices. The ΔT and GDGT/alkenone ratio were maximal during the last five deglaciations, suggesting intensified upwelling. The intensification of upwelling in the EEP coincided with those at the Peru margin and in the Southern Ocean. This coincidence suggests that the reorganization of the Southern

Hemisphere atmospheric circulation induced the intensification of the subtropical high-pressure cell, causing stronger southeast trade winds along the west coast of South America and the southern westerlies over the Southern Ocean, enhancing upwelling in both regions.

1. Introduction

The eastern equatorial Pacific (EEP) is a region between subtropical gyres of the North and South Pacific and contains the eastern terminus of the equatorial current system of the Pacific (Kessler et al., 2006). This region is important for its roles in climate variability as a result of the El Niño-Southern Oscillation (ENSO) and its significance for global carbon cycle (Fiedler and Lavin, 2006).

Glacial-interglacial changes in the oceanic condition of the EEP have been reconstructed by various studies, including of sea surface temperature (SST) (e.g., Lyle et al., 1992), salinity (e.g., Lea et al., 2000), export production (e.g., Lyle et al., 1988), and intermediate water properties (e.g., Spero and Lea, 2002; Ganeshram et al., 2000). These studies have provided evidence for an early response by the EEP to orbital forcing (e.g., Imbrie et al., 1992), and the EEP is thus thought to play an important role in amplifying climatic changes through positive feedback mechanisms.

ENSO-like variability has often been used to interpret changes in the oceanic condition of the EEP (e.g., Lea et al., 2000; Koutavas et al., 2002), but different proxy records have led to different conclusions. Some researchers, for instance, have suggested that the glacial EEP was El Niño-like based on foraminiferal Mg/Ca and $\delta^{18}O$ (e.g., Koutavas et al., 2002; Koutavas and Lynch-Stieglitz, 2003), but others have inferred a glacial La Niña-like condition (e.g., coccolith assemblages by Beaufort et al., 2001; foraminiferal assemblages by Martinez et al., 2003; alkenones by Rincon-Martinez et al., 2010). This disagreement has been attributed to differences in the behavior of different proxies (e.g., Dubois et al., 2009).

In this paper, we present temperature records derived from TEX_{86}^{H} and U^{K}_{37}' for Ocean Drilling Program (ODP) Site 1239 and interpret the U^{K}_{37}' and TEX_{86}^{H} records for the last 430,000 years. On the basis of this interpretation, we propose the difference between TEX_{86}^{H}- and U^{K}_{37}'-derived temperatures and the abundance ratio of glycerol dialkyl glycerol tetraethers (GDGTs) to alkenones as potential upwelling indices and discuss the response of the EEP upwelling system to orbital forcing.

Modern physical oceanography

The zonal surface current system in the eastern tropical Pacific (ETP) consists of westward- and eastward-flowing currents (Fig. 1). The main westward currents are the North Equatorial Current (NEC; 8°N and 20°N) and the South Equatorial Current (SEC; 3°N to 10°S). The SEC originates as a combination of the waters from the North Equatorial Counter Current (NECC), the Equatorial Undercurrent (EUC), and the Peruvian Undercurrent (Kessler, 2006) through equatorial upwelling, mixing and advection. Two main lobes of the SEC are observed at latitude of about 3°S to just north of the equator. The NECC, an eastward current flows just north of the equator and is centered at about 5°N (Wyrtki, 1967; Talley et al., 2011). This current transports warmer water from the western Pacific warm pool to the ETP region. Between the SEC and the NECC there is a narrow equatorial front (EF) that separates warm low-salinity waters in the north from cool high-salinity waters in the south (Fig. 1; Strub et al., 1998). This front is observable from July to September at about 2.5°N with a strong meridional SST gradient. In contrast, the EF position is unclear from January to April, when the southeast trades winds collapse and SST south of the Equator increases owing to reduced upwelling. The condition of the EF is correlated with the displacement of the intertropical convergence zone (ITCZ) (e.g., Pak and Zaneveld, 1974; Chelton et al., 2001; Raymond et al., 2004). The ITCZ reaches its northernmost extent in the month of August (~12°N) when southeast trade winds are stronger; the ITCZ is located closest to the equator in April (~2°N) when northeast trade winds are stronger (Waliser and Gautier, 1993).

The most influential subsurface current in this region is the EUC that flows eastward beneath the SEC. The EUC is fed by the saline New Guinea Coastal Undercurrent at its the western boundary (Talley et al., 2011) and flows within the equatorial thermocline and shoal as it approaches the Galapagos Islands (Kessler, 2006). When it reaches the Galapagos Islands, it splits into two branches (Steger et al., 1998) with the main branch flowing southward to merge with the Peruvian Undercurrent, which provides a for source of the Peru coastal upwelling (Brink et al., 1983), the other branch continues to flow eastward, merging with the NECC (Wyrtki, 1967; Fieldler and Tally, 2006; Kessler, 2006).

The EEP is a region that has been impacted by coastal upwelling. Coastal upwelling in the EEP is driven by Ekman transport generated by southeast trade winds that blow along the west coast of South America (Wrytki, 1981). The Ekman transport moves surface water offshore, away from the coastal boundary and replaces it with water from below the thermocline to maintain the mass balance. Seasonally, coastal upwelling is at its highest intensity when the strongest southeast trade winds blow over this region in boreal summer, and is reduced when southeast trade winds are relatively weak in boreal winter (Wrytki, 1975, 1981; Kessler, 2006). The seasonal variability in the EEP is superimposed by interannual El Niño events (Wang and Fiedler, 2006), which occur every 2–7 years and last for 6–18 months (Penington et al., 2006). Hydrological conditions that characterize El Niño (La Niña) phases in the EEP are a deeper (shallower) thermocline and weaker (stronger) upwelling (Kessler, 2006).

Modern observation shows a clear seasonal and interannual SST variability in the EEP region (Fig. 2a). Seasonally, higher SST is recorded during boreal winter (February), and the lowest SST is recorded in boreal summer (August). The vertical temperature gradient is larger in boreal winter than that in boreal summer. Interannually, higher SST is observed in strong El Niño years and lower SST is observed in strong La Niña years (Fig. 2a). The thermocline depth at the study site is approximately 30–50 m (Fig. 2b).

2. Materials and methods

ODP Site 1239 (0°40.32′ S, 82°4.86′ W; 1414 m water depth) is located near the eastern crest of the Carnegie Ridge and ~120 km off the coast of Ecuador (Fig. 1). The sediments are dominated by light to dark olive gray foraminifera-nannofossil ooze with varying amounts of diatoms, clay, and micrite (Mix et al., 2003). The age-depth model of this core was established by Rincon-Martinez et al. (2010) based on correlation of the $\delta^{18}O$ record of the benthic foraminifera *Cibicidoides wuellerstorfi* with the LR04 global stack (Lisiecki and Raymo, 2005). In total, 236 samples were taken from 0.02 to 14.73 meters composite depth (mcd) at 2–10 cm intervals.

Extraction and separation of lipids followed the modified method of Yamamoto et al. (2000) and Yamamoto et al. (2008). Freeze-dried and homogenized samples (~2 g) were extracted using an Accelerated Solvent Extractor 200 (ASE 200, DIONEX) with a mixture of dichloromethane and methanol (6/4 v/v) at 100°C. The extract was separated into four fractions of lipid sequences in order of polarity, F1 (3 ml hexane), F2 (3 ml 3/1 v/v hexane–toluene), F3 (4 ml toluene), and F4 (3 ml 3/1 v/v toluene–methanol), by column chromatography (SiO_2 with 5% distilled water; i.d., 5.5 mm; length, 45 mm).

The F3 fraction was analyzed with a Hewlett–Packard Model 6890 gas chromatograph with on-column injection and electronic pressure control inlet systems and a flame ionization detector (FID). Helium was used as carrier gas with the flow velocity maintained at 30 $cm.s^{-1}$. The column was a Chrompack CP-Sil5CB capillary (60 m; i.d., 0.25 mm; thickness, 0.25 μm). The oven temperature was programmed from 70 to 290°C at 20°C min^{-1}, from 290 to 310°C at 0.5°C min^{-1}, and then held for 30 min. Quantification of di- and tri-unsaturated C_{37} alkenones were achieved by comparing the peak areas with that of an internal standard (n-$C_{36}H_{74}$) on the gas chromatogram.

The alkenone unsaturation index $U^{K}_{37}{}'$ was computed from the concentrations of di-unsaturated ($C_{37:2}$MK) and tri-unsaturated ($C_{37:3}$MK) alkenones using the following equation by Prahl et al. (1988):

$$U^{K}_{37}{}' = [C_{37:2}\text{MK}] / ([C_{37:3}\text{MK}] + [C_{37:2}\text{MK}])$$

The temperature was calculated according to an equation derived by Prahl et al. (1988) based on experimental results for cultured strain 55a of *Emiliania huxleyi*:

$$U^{K}_{37}' = 0.034T + 0.039$$

where T = temperature (°C). Analytical accuracy was 0.24°C in our laboratory.

An aliquot of F4 was dissolved in hexane-2-propanol (99/1, v/v). GDGTs were analyzed using high-performance liquid chromatography–mass spectrometry (HPLC-MS) with an Agilent 1100 HPLC system connected to a Bruker Daltonics micrOTOF-HS time-of-flight mass spectrometer. Separation was conducted using a Prevail Cyano column (2.1 x 150 mm, 3μm; Alltech) maintained at 30°C following the method of Hopmans et al. (2000) and Schouten et al. (2007). Detection was achieved by atmospheric pressure positive ion chemical ionization–mass spectrometry (APCI-MS) with full scan mode (m/z 500–1500). Compounds were identified by comparing mass spectra and retention times with those of GDGT standards (formed from the main phospholipids of *Thermoplasma acidophilum* via acid hydrolysis).

Quantification was achieved by integrating the summed-peak areas in the $(M+H)^+$ and the isotopic $(M+H+1)^+$ ion traces and comparing these to the peak area of an internal standard (C_{46} GDGT) in the $(M+H)^+$ ion trace, following to the method of Huguet et al. (2006). The correction value of ionization efficiency between GDGTs and the internal standard was obtained by comparing the peak areas of *T. acidophilum*-derived mixed GDGTs and C_{46} GDGT of known amounts. The standard deviation of a replicate analysis was 3.0% of the concentration for each compound. Concentration TEX_{86}^{H} (applicable in warm water) were calculated from the concentrations of GDGT-1, GDGT-2, GDGT-3, and a regioisomer of crenarchaeol using the following expressions (Schouten et al., 2002; Kim et al., 2010):

$$TEX_{86} = ([GDGT\text{-}2] + [GDGT\text{-}3] + [Crenarchaeol\ regioisomer]) / ([GDGT\text{-}1] + [GDGT\text{-}2] + [GDGT\text{-}3] + [Crenarchaeol\ regioisomer])$$

$$TEX_{86}^{H} = \log (TEX_{86})$$

Temperature was calculated according to the following equation based on a global core-top calibration (Kim et al., 2010):

$$T = 68.4TEX_{86}^{H} + 38.6 \text{ (when } T > 15°C)$$

where T = temperature (°C). The analytical accuracy was 0.45 °C in our laboratory.

3. Results

3.1 GDGTs and TEX_{86}

The isoprenoid GDGTs detected in ODP 1239 sediments consist of caldrachaeol (GDGT-0), GDGT-1, GDGT-2, GDGT-3, crenarchaeol, and its regioisomer (Appendix I). The total concentration of isoprenoid GDGTs in sediment varied between 0.6 and 12.8 $\mu g.g^{-1}$ with an average of 5.81 $\mu g.g^{-1}$ (Fig. 3b). The relative abundances of different isoprenoid GDGTs were nearly uniform with range of 37–54% for crenarchaeol, 26–35% for caldarchaeol and 15–35% for others.

The TEX_{86}^{H}-derived temperature of the core-top sample (25.1°C) agreed with the mean annual SST at the study site (24.5°C, Locarnini et al., 2010). TEX_{86}^{H}-derived SST varied between 20.2 and 27.2°C and was generally higher during interglacials and lower during glacials (Fig. 3a).

The branched isoprenoid tetraether (BIT) index, an indicator of soil bacteria contribution (see Hopmans et al., 2004), varied between 0.01 and 0.06 (Fig. 3d) suggesting a low contribution of soil organic matter in the study samples. Weijers et al. (2006) noted that samples having high BIT (>0.4) may show anomalously high TEX_{86}^{H}-derived temperatures, but this concern was not relevant for the samples used in this study.

3.2. Alkenones and $U^{K}_{37}{}'$

The total concentration of C_{37}-C_{39} alkenones in sediment varied between 0.5 and 28.7 μg.g^{-1} with an average of 8.9 μg.g^{-1} (Fig. 3b). The alkenone concentration tended to be higher in the interval between 400 ka and 240 ka than in the intervals between 430 and 400 ka and between 240 and 0 ka.

The $U^{K}_{37}{}'$-derived temperature of the core-top sample (25.6°C) agreed with the mean annual SST. $U^{K}_{37}{}'$-derived SST varied between 21.5 and 26.6°C and was generally higher in interglacials and lower in glacials (Fig. 3a). The $U^{K}_{37}{}'$ record obtained in this study was nearly identical to a record for the study site by Rincon-Martinez et al. (2010).

4. Discussion

4.1. Difference in proxy-derived temperatures

The variation of TEX_{86}^{H}-derived temperature is roughly consistent with those of the $U^{K}_{37}{}'$-derived temperature at the study site (Fig. 3a), but significant difference was observed in the intervals of late MIS 11, and MIS 10, and MIS-6 when the $U^{K}_{37}{}'$-derived temperature was a maximum of 5.5°C higher than the TEX_{86}^{H}-derived temperature (Fig. 3a).

Dubois et al. (2009) and Kienast et al. (2012) assumed that $U^{K}_{37}{}'$ reflects mean annual SST because the $U^{K}_{37}{}'$-derived temperature in EEP core-top sediments corresponded to mean annual SST. A sediment trap study at two sites in the central tropical Pacific showed no significant difference in the sinking flux of alkenone producers (*Emiliania huxleyi* and *Gephyrocapsa oceanica*) between strong and weak El Niño periods (Broerse, 2000), suggesting that the production of alkenone is not sensitive to upwelling intensity. We thus assume that $U^{K}_{37}{}'$ does reflect the mean annual SST at the study site.

The behavior of Thaumarchaeota and the production of GDGTs are not fully clear in the EEP. Thaumarchaeota (GDGTs producer) are ubiquitous and abundant throughout the seawater column (e.g., Massana et al., 2000; Karner et al., 2001). In the central equatorial Pacific, GDGTs are mainly produced in the thermocline layer (TL) (Turich et al., 2007). Recent case studies assumed that the TEX_{86}^{H}-derived temperatures in EEP sediments reflect the temperature of the thermocline (30–50 m) rather than SSTs (Ho et al., 2011; Seki et al., 2012). Thaumarchaeota in marine environments have been recognized to be both heterotrophs (e.g., Ouverney and Fuhrman, 2000; Agogué et al., 2008; Zhang et al., 2009) and chemoautotrophic nitrifiers (e.g., Könneke et al., 2005; Hallam et al., 2006). Organic matter and NH_3 are produced by phytoplankton and by the decay of organic matter in surface and subsurface water, which explains why Thaumarchaeota are produced in both the surface mixed layer (SML) and TL. We thus assume that TEX_{86}^{H} reflects a mixed temperature signal from the SML and TL (Fig.4). The production of Thaumarchaeota is fueled by the supply of organic matter and NH_3. Both are more enhanced by phytoplankton production in upwelling periods. Yamamoto et al. (2012) observed that enhanced sinking flux of GDGTs is linked with phytoplankton bloom in the mid-latitude northwestern Pacific. GDGT abundance thus may reflect primary production and upwelling intensity.

TEX_{86}^{H} showed higher temperatures than U^{K}_{37}' during the some deglaciations (Fig. 3a), but this does not mean that the integrated SST of the SML and TL was higher than the SST of the SML. The calibration of TEX_{86}^{H} to SST was conducted by comparing core-top TEX_{86}^{H} with mean annual SST (Kim et al., 2010). If the phenomenon of TEX_{86}^{H} recording both the SST and thermocline temperatures is common in tropical oceans, then calibration requires a comparison between core top TEX_{86}^{H} and integrated temperatures of the SML and TL; this calibration should give cooler estimates. The temperature reversal during the last deglaciation is thus attributed to the overestimation of TEX_{86}^{H}-derived temperature.

4.2. GDGT/alkenone ratio and ΔT as upwelling indices

The relative abundance of isoprenoid GDGTs to alkenones (GDGT/alkenone ratio) was enhanced during the last five deglaciations (Fig. 5a), suggesting an enhanced production of GDGTs. When upwelling intensifies, GDGT production increases due to increasing NH_3 and organic matter. In contrast, when upwelling weakens, GDGT production decreases. The GDGT/alkenone ratio can thus be used as an index of upwelling intensity.

The difference between TEX_{86}^{H}- and U^{K}_{37}'-derived temperatures (ΔT) was computed by subtracting U^{K}_{37}'-derived SST from TEX_{86}^{H}-derived temperature ($\Delta T = TEX_{86}^{H} - U^{K}_{37}'$). U^{K}_{37}' reflects the temperature of the SML and TEX_{86}^{H} reflects integrated temperatures from the SML and the TL. When upwelling intensifies, the temperature gradient between the SML and TL decreases (Fig. 4), and ΔT shifts in a positive direction. In contrast, when upwelling weakens, the temperature gradient between the SML and TL increases, and ΔT shifts in a negative direction. We thus assume that ΔT is a potential index of upwelling intensity.

ΔT varied between -6.2 and 4.1°C and showed maxima at 15, 50, 127, 213, 243, 260, 274, 310, 330, 340 and 427 ka. The maxima at 15, 127, 243, 340, and 427 ka correspond to glacial terminations (Fig. 5a). Minimal peaks of ΔT occurred at 33, 86, 179, 237, 289, and 386 ka. The variation in ΔT is very similar to that in the GDGT/alkenone ratio, although there are some mismatches in MIS 8 and MIS 11. This correspondence suggests that both are robust indices of upwelling intensity.

Positive ΔT and an elevated GDGT/alkenone ratio at the study site during deglaciations are associated with heavier $\delta^{18}O$ of subsurface-dwelling foraminifera (Pena et al., 2008) and increased export production (Pedersen, 1983; Lyle et al., 1988; Kienast et al., 2006) in the EEP. Pena et al. (2008) showed that thermocline water $\delta^{18}O$ (DT-$\delta^{18}O_{sw}$) at ODP Site 1240, reconstructed from the subsurface-dwelling foraminifera *Neogloboquadrina dutertrei*, was maximized during the last three deglaciations (Fig. 5d). This suggests intensified upwelling in those periods. Abrupt increases in organic carbon content during deglaciations were reported from sites P6 (Pedersen, 1983), V19-28 (Lyle et al., 1988), and ME0005A-24JC and 27JC (Kienast et al., 2006) in the EEP (Fig. 5b), suggesting that export production was maximized during the last two deglaciations. The elevated ΔT and GDGT/alkenone ratio at the study site indicate not only the intensification of local upwelling, but also the intensification of regional upwelling associated with thermocline shoaling and enhanced export production in the EEP during deglaciations.

4.3. Hydrological evolution in the EEP

The ΔT record mirrors sedimentary $\delta^{15}N$ records from the Peru margin (Fig. 5c), which have been suggested to reflect the intensity of denitrification regulated by Peruvian coastal upwelling (Ganeshram et al., 2000). The trend in $\delta^{15}N$ at the Peru margin was slightly different from those in the EEP (Dubois and Kienast, 2011) and at the Mexican margin (Ganeshram et al., 2000) (Fig. 5c). The maxima of $\delta^{15}N$ at terminations are significant at the Peru margin but not in the EEP or at the Mexican margin, suggesting that $\delta^{15}N$ in the eastern Pacific margin was determined by the denitrification in the Peru margin and modified by local factors (Robinson et al., 2009). The correspondence between ΔT and the Peru margin $\delta^{15}N$ records suggests that the upwelling at the study site was closely linked with Peruvian coastal upwelling. The study site is located in a region influenced by the coastal upwelling system (Wrytki, 1981; Pennington et al., 2006; Talley et al., 2011). Because the southeast trade winds are a principal agent driving coastal upwelling along the west coast of South American continent (Wrytki, 1981;

Kessler, 2006), it is highly likely that the southeast trade winds intensified during deglaciations owing to the stronger South Pacific High.

The paleo-position of the ITCZ was approximated using dust fluxes across the equator over the last 30 ka (McGee et al., 2007). The results of that analysis suggest that the ITCZ did not shift southward during the last deglaciation. Xie and Marcantonio (2012) precisely estimated the paleo-position of the ITCZ using neodymium isotopes (ε_{Nd}) derived from transect dust obtained by McGee et al. (2007). The average ε_{Nd} values from the last glacial and Holocene show similar gradients throughout the equatorial transect, but the latitudinal gradient was stronger, and a steeper interval was evident during the last deglaciation between 5°N and 7°N. This suggests more northerly mean position of the ITCZ.

Yamamoto et al. (2007) reconstructed the intensity of the California Current during the last 150,000 years and showed that the subtropical high-pressure cell in the North Pacific weakened during the last two deglaciations. Lyle et al. (2012) suggested that high precipitation in the Great Basin of the western United States during the last deglaciation was not caused by the southward shift of westerly storms, but instead by the northward transport of moist air masses from the tropical Pacific because of the weaker North Pacific High. This presumes that the northeast trade winds were not intensified under the condition of the weaker North Pacific High.

The stronger South Pacific High, combined with the weaker North Pacific High and northward shift of the ITCZ during the last deglaciation was an asymmetrical atmospheric phenomenon between the Northern and Southern hemispheres. This anti-phase variation in the subtropical high-pressure cells of both hemispheres was presumably caused by changes in the heat balance between the hemispheres (Fig. 6).

The ENSO model has been applied to understand hydrological evolution of the EEP (e.g., Lea et al., 2000; Koutavas et al., 2002; Koutavas and Lynch-Stieglitz, 2003; Martinez et al., 2003; Pena et al., 2008; Rincon-Martinez et al., 2010). Pena et al. (2008) proposed the deep thermocline seawater $\delta^{18}O$ (DT-$\delta^{18}O_{sw}$) based on *Neogloboquadrina dutertrei* $\delta^{18}O$ at Site 1240 and suggested that EEP hydrology was characterized by a La Niña-like condition during deglaciations. However, the zonal gradient of SST was inconsistent with a La Niña-like state during the last deglaciation (Fig. 5e). The DT-$\delta^{18}O_{sw}$ at ODP Site 1240 showed maximum peaks during deglaciations (Pena et al., 2008), but the Mg/Ca-SST, between the western and eastern Pacific did not show a large temperature gradient typical of La Niña (Lea et al., 2000). Also, the weaker North Pacific High evidenced during the last deglaciation (Yamamoto et al., 2007; Lyle et al., 2012) is not consistent with a La Niña-like state; a weaker North Pacific High is typical of the modern El Niño condition (Bogad and Lynn, 2001). We thus suggest that intensified upwelling shown by enhanced DT-$\delta^{18}O_{sw}$ at Site 1240 was not linked to a La Niña-like state, and an ENSO analogy cannot to be applied to explain hydrological conditions in the Pacific during the last deglaciation.

The intensification of upwelling in the EEP and the Peru margin during the last deglaciation coincided with intensification of upwelling in the Southern Ocean (Toggweiler et al., 2006; Anderson et al., 2009). Because upwelling in the Southern Ocean is regulated by the position of the southern westerlies (Russell et al., 2006; Toggweiler et al., 2006), the synchronous intensification of upwelling systems in the EEP, the Peru margin, and the Southern Ocean suggests that the reorganization of atmospheric circulation in the Southern Hemisphere induced the intensification of the subtropical high-pressure cell, causing stronger southeast trade winds along the west coast of South America and southern westerlies over the Southern Ocean, enhancing upwelling in both regions.

The intensification of the South Pacific High caused southern westerlies to move poleward and the ITCZ to shift northward during deglaciations (Fig. 6). In response, the center of upwelling moved northward and cold tongue upwelling in the EEP area intensified. The stronger South Pacific High during the last deglaciation caused a drier climate in the Patagonia region of South America (de Porras et al., 2012), and the weaker North Pacific High caused a wetter climate in the Great Basin of the western United States (Lyle et al., 2012). This perspective is useful for understanding the hydrological and climatological evolution of the eastern Pacific region.

5. Conclusions

The abundance ratio of GDGTs to alkenone (GDGT/alkenone ratio) and difference between TEX_{86}^{H}- and $U^{K}_{37}{'}$-derived temperature (ΔT) can be used as upwelling indices in the EEP. Our new data show that intensification of upwelling occurred in the EEP at each of the last five glacial terminations. The result suggests that the intensification of upwelling was a common phenomenon in the EEP at glacial terminations. The similar timing of intensified upwelling in the EEP, the Peru margin, and the Southern Ocean suggests an intensification of the South Pacific High during deglaciations. This new perspective can help explain the hydrological evolution of the eastern Pacific region during deglaciations.

Acknowledgements

The Ocean Drilling Program Leg 202 provided the samples used in this study. We thank Daniel Rincon Martinez for providing us with data on the age and foraminiferal oxygen isotopes of the study core. We also thank Patrizia Ziveri, Alexandra Broerse, and Kyoko Hagino for providing information on coccolithophores in the EEP, Leopoldo Pena for data regarding the thermocline water $\delta^{18}O$ from ODP Site 1240, Eric Galbraith for data of $\delta^{15}N$ records from core NH22P and CD38-02, and Tatsufumi Okino, Keiko Ohnishi and Tadamichi Oba for their analytical assistance.

References

Agogué, H., Brink, M., Dinasquet, J., Herndl, G.J., 2008. Major gradients in putatively nitrifying and non-nitrifying Archaea in the deep North Atlantic. Nature 456, 788–792.

Anderson, R.F., Ali, S., Bradtmiller, L.I., Nielsen, S.H.H., Fleisher, M.Q., Anderson, B.E., Burckle, L.H., 2009. Wind-driven upwelling in the Southern Ocean and the deglacial rise in atmospheric CO_2. Science 323, 1443–1448.

Beaufort, L., de Garidel-Thoron, T., Mix, A.C., Pisias, N.G., 2001. ENSO-like forcing on oceanic primary production during the late Pleistocene. Science 293, 2440–2444.

Bograd, S., Lynn, R.J., 2001. Physical-biological coupling in the California Current during the 1997–99 El Niño-La Niña cycle. Geophysical Research Letters 28, 275–278.

Brink, K.H., Halpern, D., Huyer, A., Smith, R.L., 1983. The physical environment of the

Peruvian upwelling system. Progress in Oceanography 12, 285–305.

Broerse, A.T.C., 2000. Coccolithophore export production in the selected ocean environments, Ph.D. thesis, Faculty of Earth Science, Vrije Universiteit, Amsterdam, Netherlands.

Chelton, D.B., Esbensen, S.K.. Schlax, M.G., Thum, N., Freilich, M.H., Wentz, F.J., Gentemann, C.L., McPhaden, M.J. Schopf, P.S., 2001. Observations of coupling between surface wind stress and sea surface temperature in the eastern tropical Pacific. Journal of Climate 14, 1479–1498.

de Porras, M.E., Maldonado, A, Abarzúa, A.M., Cárdenas, M.L., Francois, J.P., Martel-Cea, A., Stern, C.R., Méndez, C., Reyes, O., 2012. Postglacial vegetation, fire and climate dynamics at Central Chilean Patagonia (Lake Shaman, 44°S). Quaternary Science Reviews 50, 71–85.

Dubois, N., Kienast, M., Normandeau, C. Herbert, T.D., 2009. Eastern equatorial Pacific cold tongue during the last glacial maximum as seen from alkenone paleothermometry. Paleoceanography 24, PA4207.

Dubois, N., Kienast, M., 2011. Spatial reorganization in the equatorial divergence in the eastern tropical Pacific during the last 150 kyr. Geophysical Research Letters 38, L16606.

Fiedler, P.C., Lavin, M.F., 2006. Introduction: a review of eastern tropical Pacific oceanography. Progress in Oceanography 69, 94–100.

Fiedler, P.C., Talley, L.D., 2006. Hydrography of the eastern tropical Pacific: a review. Progress in Oceanography 69 (2–4), 143–180.

Ganeshram, R.S., Pedersen, T.F., Calvert, S.E., McNeil, G.W., Fontugne, M.R., 2000. Glacial-interglacial variability in denitrification in the world's oceans: causes and consequences. Paleoceanography 15, 361–376.

Hallam, S.J., Mincer, T.J., Schleper, C., Preston, C.M., Roberts, K., Richardson, P.M., DeLong, E.F., 2006. Pathway of carbon assimilation and ammonia oxidation suggested by environmental genomic analyses of marine Crenarchaeota. PLoS Biology 4, 520–536.

Ho, S. L., Yamamoto, M., Mollenhauer, G., Minagawa M., 2011. Core top TEX_{86} values in the south and equatorial Pacific. Organic Geochemistry 42, 94–99.

Hopmans, E.C., Schouten, S., Pancost, R., van der Meer, M.T.J., Sinninghe Damsté, J.S., 2000. Analysis of intact tetraether lipids in archaeal cell material and sediments by high performance liquid chromatography/atmospheric pressure chemical ionization mass spectrometry. Rapid Communications in Mass Spectrometry 14, 585–589.

Hopmans E.C., Weijers, J.W.H., Schefuß, E., Herfort, L., Sinninghe Damsté, J.S., Schouten, S., 2004. A novel proxy for terrestrial organic matter in sediments based on branched and isoprenoid tetraether lipids. Earth and Planetary Science Letters 224, 107–116.

Huguet, C., Hopmans, E.C., Febo-Ayala, W., Thompson, D.H., Sinninghe Damsté, J.S., Schouten, S., 2006. An improved method to determine the absolute abundance of glycerol dibiphytanyl glycerol tetraether lipids. Organic Geochemistry 37, 1036–1041.

Imbrie, J., Boyle, E.A., Clemens, S.C., Duffy, A., Howard, W.R., Kukla, G., Kutzbach, J., Martinson, D.G., McIntyre, A., Mix, A.C., Molfino, B., Morley, J.J., Peterson, L.C., Pisias, N.G., Prell, W.L., Raymo, M.E., Shackleton, N.J., Toggweiler, J.R., 1992. On the structure and origin of major glaciation cycles. I. Linear responses to Milankovitch forcing. Paleoceanography 7, 701–738.

Karner, M.B., DeLong, E.F., Karl, D.M., 2001. Archaeal dominance in the esopelagic zone of the Pacific Ocean. Nature 409, 507–510.

Kessler, W.S., 2006. The circulation of the eastern tropical Pacific: a review. Progress in Oceanography 69, 181–217.

Kienast, M., Kienast, S., Calvert, S., Eglinton, T., Mollenhauer, G., Francois, R., Mix, A., 2006. Eastern Pacific cooling and Atlantic overturning circulation during the last deglaciation. Nature 443, 846–849.

Kienast, M., MacIntyre, G., Dubois, N., Higginson, S., Normandeau, C., Chazen C.R., 2012. Alkenone unsaturation in surface sediments from the eastern equatorial Pacific: Implications for SST reconstructions. Paleoceanography 27, PA1210.

Kim, J.H., van der Meer, J., Schouten, S., Helmke, P., Willmott, V., Sangiorgi, F., Koc, N., Hopmans, E.C., Sinninghe Damsté, J.S., 2010. New indices and calibrations derived from the distribution of crenarchaeol isoprenoid tetraether lipids: implications for past sea surface temperature reconstructions. Geochimica et Cosmochimica Acta 74, 4639–4654.

Könneke, M., Bernhard, A.E., de la Torre, J.R., Walker, C.B., Waterbury, J.B., Stahl, D.A., 2005. Isolation of an autotrophic ammonia-oxidizing archaeon. Nature 437, 543–546.

Koutavas, A., Lynch-Stieglitz, J., 2003. Glacial-interglacial dynamics of the eastern equatorial Pacific cold tongue. Intertropical Convergence Zone system reconstructed from oxygen isotope records. Paleoceanography 18, 1089.

Koutavas, A., Lynch-Stieglitz, J., Marchitto, T.M., Sachs, J.P., 2002. El Niño-like pattern in ice age tropical Pacific sea surface temperature. Science 297, 226–230.

Lea, D.W., Pak, D.K., Spero, H.J., 2000. Climate impact of late quaternary equatorial Pacific sea surface temperature variations. Science 289, 1719–1724.

Lisiecki, L.E., Raymo, M.E., 2005. A Pliocene-Pleistocene stack of 57 globally distributed benthic $\delta^{18}O$ records. Paleoceanography 20, PA1003.

Locarnini, R.A., Mishonov, A.V., Antonov, J.I., Boyer, T.P., Garcia, H.E., Baranova, O. K., Zweng, M.M., Johnson, D.R., 2010. In: Levitus, S. (Ed.), World Ocean Atlas 2009, 1, Temperature, NOAA Atlas NESDIS, 68, U.S. Government Printing Office, Washington, D.C., pp. 184.

Lyle, M., Murray, D.W., Finney, B.P., Dymond, J., Pobbins, J.M., Brooksforce, K., 1988. The record of Late Pleistocene biogenic sedimentation in the eastern tropical Pacific Ocean. Paleoceanography 3, 39–59.

Lyle, M., Prahl, F.G., Sparrow M.A., 1992. Upwelling and productivity changes inferred from a temperature record in the central equatorial Pacific. Nature 355, 812–815.

Lyle, M., Heusser, L., Ravelo, C., Yamamoto, M., Barron, J., Diffenbaugh, N.S., Herbert, T., Andreasen, D., 2012. Out of the Tropics: The Pacific, Great Basin Lakes, and Late Pleistocene water cycle in the western United States. Science 337, 1629–1633.

Martinez, I., Keigwin, L., Barrows, T.T., Yokoyama, Y., Southon, J., 2003. La Niña-like conditions in the eastern equatorial Pacific and a stronger Choco jet in the northern Andes during the last glaciations. Paleoceanography 18, 1033.

Massana, R., Delong, E. F., Pedros-Alio, C., Murray, A. E. Preston, C. M. ,2000. A few cosmopolitan phylotypes dominate planktonic archaeal assemblages in widely different oceanic provinces. Applied of Environmental Microbiology 66, 1777–1787.

Medina-Elizalde, M., Lea, D.W., 2005. The Mid-Pleistocene transition in the tropical Pacific. Science 310, 1009–1012.

McGee, D., Marcantonio F., Lynch-Stieglitz, J., 2007. Deglacial changes in dust flux into the eastern equatorial Pacific. Earth and Planetary Science Letters 257, 215–230.

Mix, A.C., Tiedemann, R., Blum, P., et al., 2003. Proceeding of the Ocean Drilling Program, Initial Reports, 202: College Station, TX (Ocean Drilling Program), 1–93.

Ouverney, C.C., Fuhrman, J.A., 2000. Marine planktonic archaea take up amino acids. Applied Environmental Microbiology 66, 4829–4833.

Paillard, D., Labeyrie, L., Yiou, P., 1996. Macintosh program performs time-series analysis. Eos Transaction AGU 77, 379.

Pak, H., Zaneveld, J.R.V., 1974. Equatorial front in the eastern Pacific Ocean. Journal of Physical Oceanography 4, 570–578.

Pedersen, T.F., 1983. Increased productivity in the eastern equatorial Pacific during the last glacial maximum (19,000 to 14,000 yr. B.P.). Geology 11, 16–19.

Pena, L.D., Cacho, I., Ferretti, P., Hall, M.A., 2008. El Niño-Southern Oscillation-like variability during glacial terminations and interlatitudinal tele-connections. Paleoceanography 23, PA3101.

Pennington, J.T., Mahoney, K.L., Kuwahara, V.S., Kolber, D.D., Calienes, R., Chavez, F.P., 2006. Primary production in the eastern tropical Pacific: a review. Progress in Oceanography 69 (2 – 4), 285–317.

Prahl, F.G., Muehlhausen, L.A., Zahnke, D.L., 1988. Further evaluation of long chain alkenones as indicators of paleoceanographic conditions. Geochimica et Cosmochimica Acta 52, 2303–2310.

Raymond, D.J., Esbensen, S.K., Paulson, C., Gregg, M., Bretherton, C.S., Petersen, W.A., Cifelli, R., Shay, L.K., Ohlmann, C., Zudeima, P., 2004. EPIC2001 and the coupled ocean-atmosphere system of the tropical east Pacific. Bulletin of American Meteorological Society 85, 1341–1354.

Reynolds, R.W., Rayner, N.A., Smith, T.M., Stokes, D.C., Wang, W., 2002. An improved in situ and satellite SST analysis for climate. Journal of Climate 15, 1609–1625. <http://iridl.ldeo.columbia.edu/SOURCES/.NOAA/.NCEP/.EMC/.CMB/.GLOBAL/.Reyn_SmithOIv2/.monthly/>

Rincon-Martínez, D., Lamy, F., Contreras, S., Leduc, G., Bard, E., Saukel, C., Blaz, T., Mackensen, A., Tiedeman, R., 2010. More humid interglacials in Ecuador during the past 500 kyr linked to latitudinal shifts of the equatorial front and Intertropical Convergence Zone in the eastern equatorial Pacific. Paleoceanography 25, PA2210.

Robinson, R.S., Martinez, P., Pena, L.D., Cacho, I., 2009. Nitrogen isotopic evidence for deglacial changes in nutrient supply in the eastern equatorial Pacific. Paleoceanography 24, PA4213.

Russell, J.L., Dixon, K.W., Gnanadesikan, A., Stouffer, R.J., Toggweiler, J.R., 2006. The Southern hemisphere westerlies in a warming world: propping open the door to the deep ocean. Journal of Climate 19, 6382–6390.

Schouten, S., Hopmans, E.C., Schefuß, E., Sinninghe Damsté, J.S., 2002. Distributional variations in marine crenarchaeotal membrane lipids: a new organic proxy for reconstructing ancient sea water temperatures? Earth and Planetary Science Letters 204, 265–274.

Schouten, S, Hudget, C., Hopmans, E.C., Kienhuis, M.V.M., Sinninghe Damsté, J.S., 2007. Analytical methodology for TEX_{86} paleothermometry by high performance liquid chromatography/atmospheric pressure chemical ionization-mass spectrometry. Analytical Chemistry 79, 2940–2944.

Seki, O., Schmidt, D.N., Schouten, S., Hopmans, E.C., Sinninghe Damsté, J.S., Pancost, R.D., 2012. Paleoceanographic changes in the eastern equatorial Pacific over the last 10 Myr. Paleoceanography 27, PA3224.

Spero, H.J., Lea, D.W., 2002. The cause of carbon isotope minimum events on glacial terminations. Science 296, 522–525.

Steger, J.M., Collins, C.A., Chu P.C., 1998. Circulation in the Archipielago de Colon (Galápagos Islands). Deep-Sea Research II 45, 1093–1114.

Strub, P.T., Mesias, J.M., Montecino, V., Rutllant, J., Salinas, S., 1998. Coastal ocean circulation off western South America. In: Robinson, A.R., Brink, K.H. (Eds.), The Sea, Ideas and Observations on Progress in the Study of the Seas, Vol. 11, Global Coastal Ocean Regional Studies and Syntheses. Wiley, New York, pp. 273–313.

Talley, L.D., Pickard, G.L., Emery, W.J., Swift, J.H., 2011. Descriptive physical oceanography. 6th Edition. Elsevier, Boston.

Toggweiler, J.R., Russell, J.L., Carson, S., 2006. Midlatitude westerlies, atmospheric CO_2, and climate change during the ice ages. Paleoceanography 21, PA2005.

Trenberth, K.E., 1997. The definition of El Niño. Bulletin of the American Meteorological Society 78, 2771–2777.

Turich, C., Freeman, K.H., Bruns, M.A., Conte, M., Jones, A.D. and Wakeham, S.G., 2007. Lipids of marine Archaea: Patterns and provenance in the water-column and sediments. Geochimica et Cosmochimica Acta 71, 3272–3291.

Waliser, D.E., Gautier, C., 1993, A satellite-derived climatology of the ITCZ. Journal of Climate 6, 2162–2174.

Wang, C., Fiedler, P.C., 2006. ENSO variability in the eastern tropical Pacific: a review. Progress in Oceanography 69 (2–4), 239–266.

Weijers, J.W.H., Schouten, S., Spaargaren, O.C., Sinninghe Damsté, J.S., 2006. Occurrence and distribution of tetraether membrane in soils: implications for the use of the BIT index and the TEX_{86} SST proxy. Organic Geochemistry 37, 1680–1693.

Wyrtki, K., 1967. Circulation and water masses in the eastern equatorial Pacific Ocean. International Journal of Oceanology and Limnology 1, 117–147.

Wyrtki, K., 1975. El Niño – The dynamic response of the equatorial Pacific Ocean to atmospheric forcing. Journal of Physical Oceanography 5, 572–584.

Wyrtki, K., 1981. An estimate of equatorial upwelling in the Pacific. Journal of Physical Oceanography 11, 1205–1214.

Xie, R.C., Marcantonio, F., 2012. Deglacial dust provenance changes in the eastern equatorial Pacific and implications for ITCZ movement. Earth and Planetary Science Letters 317-318, 386–395.

Yamamoto, M., Shiraiwa, Y., Inouye, I., 2000. Physiological responses of lipids in *Emiliania huxleyi* and *Gephyrocapsa oceanica* (Haptophyceae) to growth status and their implications for alkenone paleothermometry. Organic Geochemistry 31, 799–811.

Yamamoto, M., Yamamuro, M., Tanaka, Y., 2007. The California current system during the last 136,000 years: response of the North Pacific High to precessional forcing. Quatenary Science Reviews 26, 405–414.

Yamamoto, M., Okino, T., Sugisaki, S., Sakamoto, T., 2008. Late Pleistocene changes in terrestrial biomarkers in sediments from the central Arctic Ocean. Organic Geochemistry 39, 754–763.

Yamamoto, M., Shimamoto, A., Fukuhara, T., Tanaka, Y., Ishizaka, J., 2012. Glycerol dialkyl glycerol tetraethers and TEX_{86} index in sinking particles in the western North Pacific. Organic Geochemistry 53, 52–62.

Zhang, Y., Sintes, E., Chen, J., Zhnag, Y., Dai, M., Jiao, N., Herndl, G.J., 2009. Role of mesoscale cyclonic eddies in the distribution and activity of Archaea and bacteria in the South China Sea. Aquatic Microbial Ecology 56, 65–79.

Figure

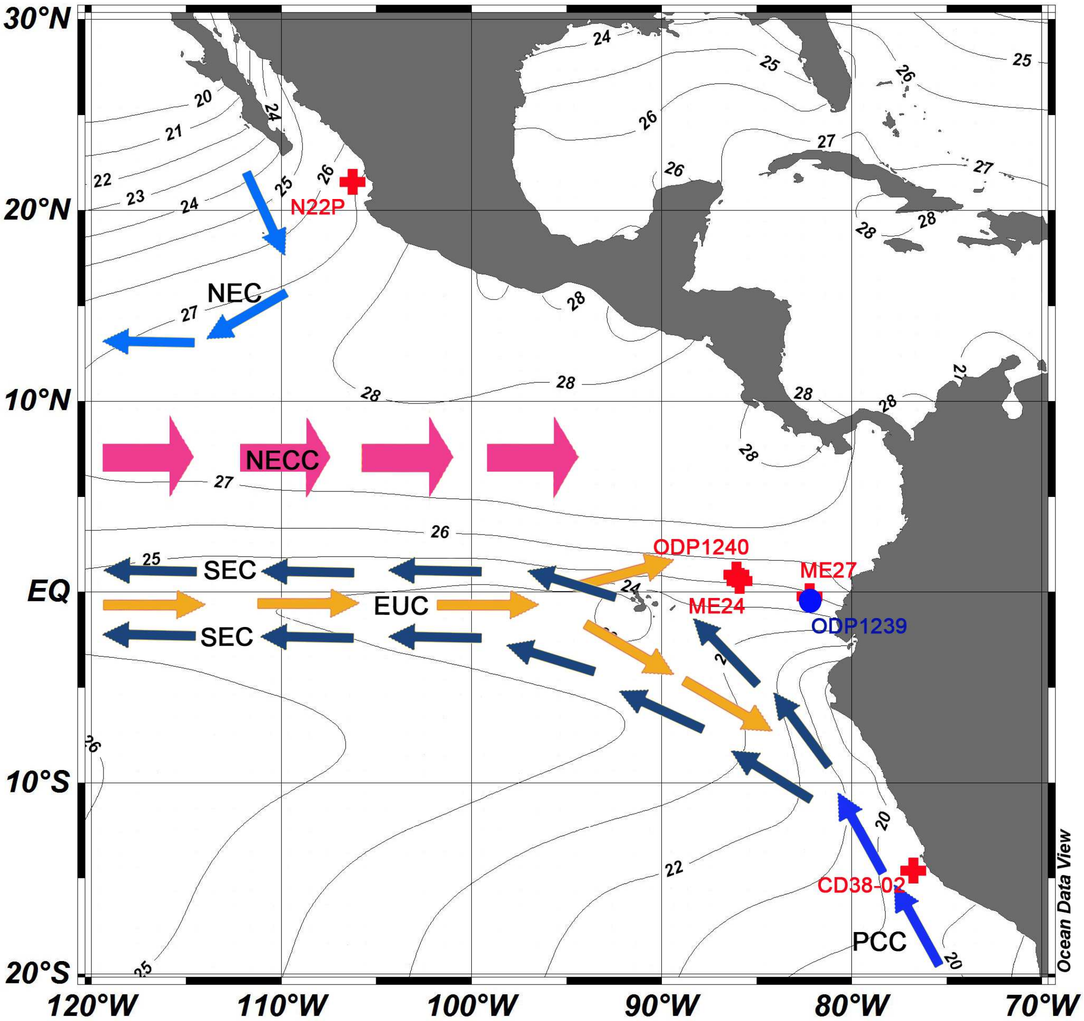

Figure 1. Map showing mean annual SST (Locarnini et al., 2010), the location of ODP Site 1239 (this study), Sites 1240, ME24, ME27, N22P, CD38-02 and the surface and subsurface ocean currents in the EEP. SEC = South Equatorial Current, NEC = North Equatorial Current, EUC = Equatorial Undercurrent, NECC = North Equatorial Countercurrent; modified after Kessler (2006) and Pennington et al. (2006).

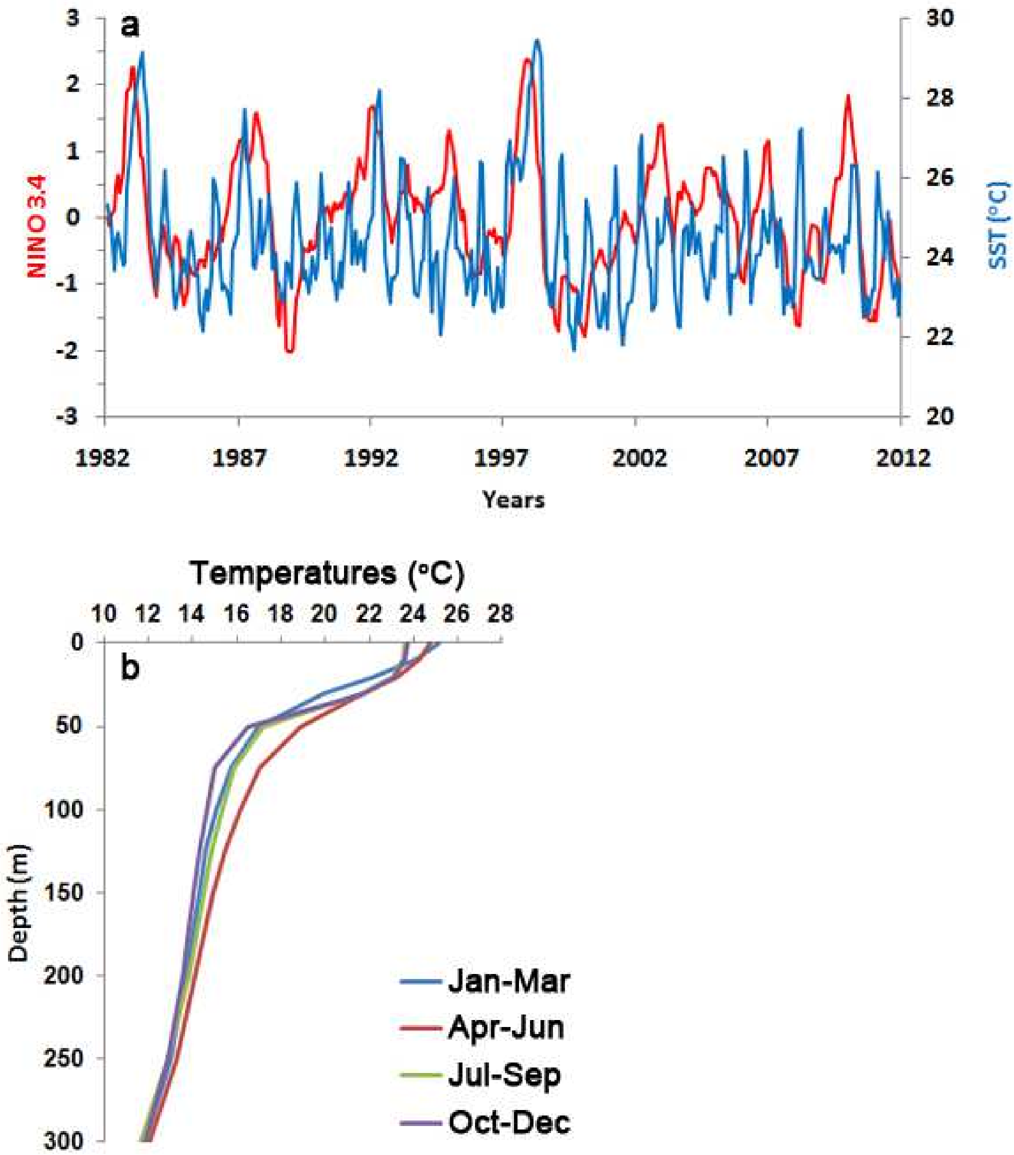

Figure 2. Records of (a) Niño 3.4 index (averaged SST anomaly in the region 170°W–120°W, 5°S–5°N) (Trenberth, 1997) and monthly SST at 0.5°S, 82.5°W (Reynolds et al., 2002) from January 1982 to December 2011 (see online data at http://iridl.ldeo.columbia.edu/SOURCES/.NOAA/.NCEP/.EMC/.CMB/.GLOBAL/.Reyn_SmithOIv2/.monthly/ for detail); (b) Seasonal vertical water structure at 0.5°S, 82.5°W (see online data at http://iridl.ldeo.columbia.edu/SOURCES/.LEVITUS94/.MONTHLY/.temp/)

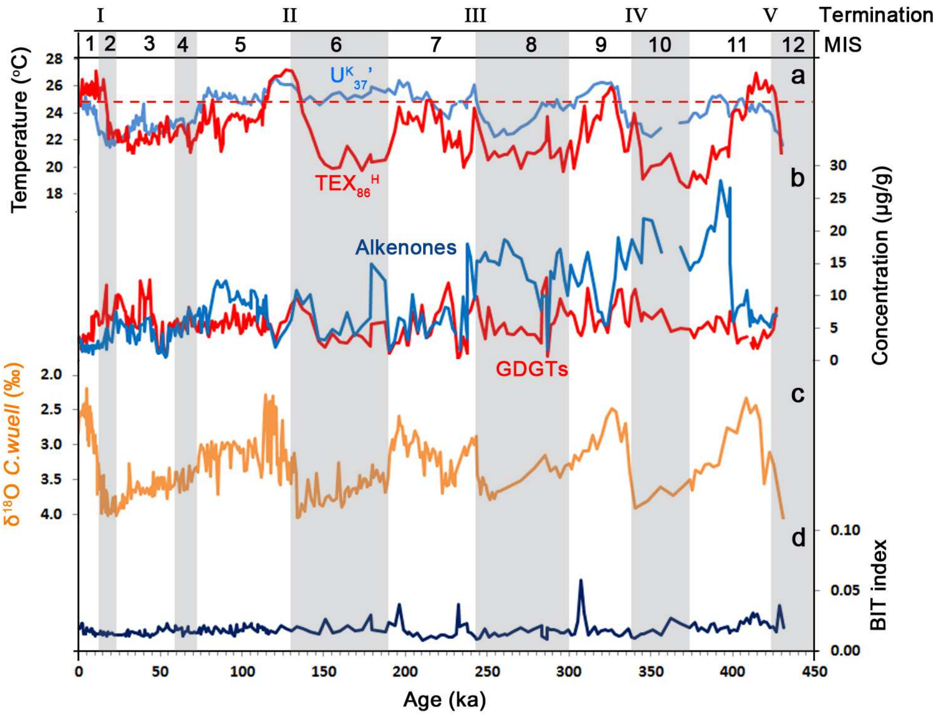

Figure 3. Variations in (a) TEX_{86}^{H}- and U^{K}_{37}′-derived temperatures; (b) the concentration of alkenones and isoprenoid GDGTs; (c) $\delta^{18}O$ of the benthic foraminifera *C. wuellerstorfi* at the study site (Rincon-Martinez et al., 2010); (d) branched isoprenoid tetraether (BIT) index.

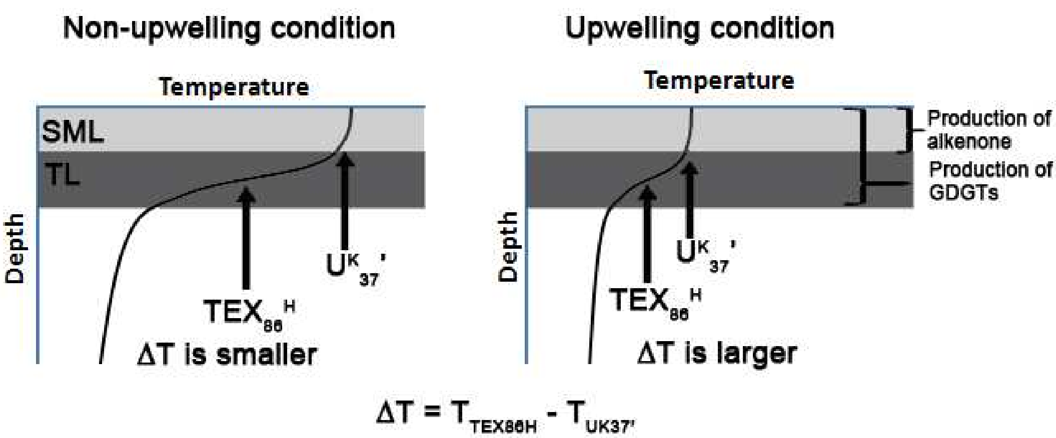

Figure 4. Conceptual model of ΔT in upwelling and non-upwelling conditions.

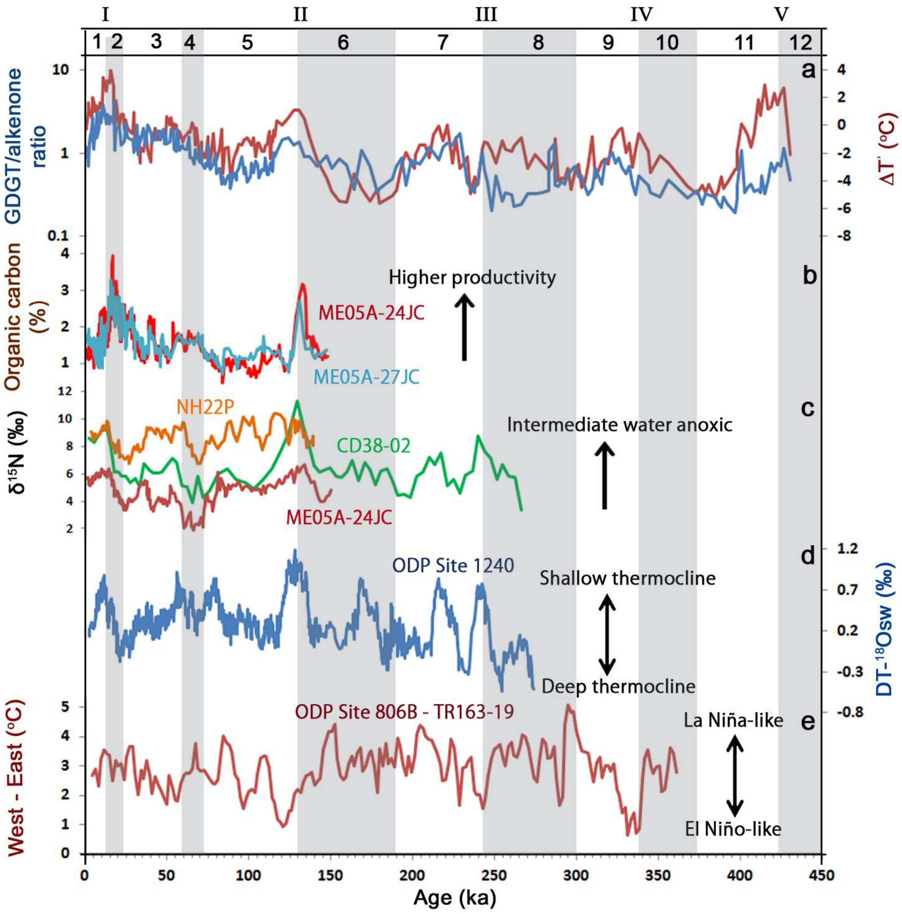

Figure 5. Variation in (a) the difference between TEX_{86}^{H} and U^{K}_{37}' temperatures (ΔT) and the abundance ratio of GDGTs to alkenones (GDGT/alkenone); (b) organic carbon content at ME0005A-24JC and ME0005A-27JC (Dubois and Kienast, 2011); (c) $\delta^{15}N$ of bulk sediments from cores CD38-02 and NH22P at the Peru and Mexican margins, respectively (Ganeshram et al., 2000) and core ME0005A-27JC in the EEP (Dubois and Kienast, 2011); (d) DT-$\delta^{18}O_{sw}$ at ODP Site 1240 (Pena et al., 2008); (e) Mg/Ca-derived temperature difference (smoothed; west-east) between the western equatorial Pacific

(ODP Site 806B; Medina-Elizalde and Lea, 2005) and the EEP (core TR163-19; Lea et al., 2000).

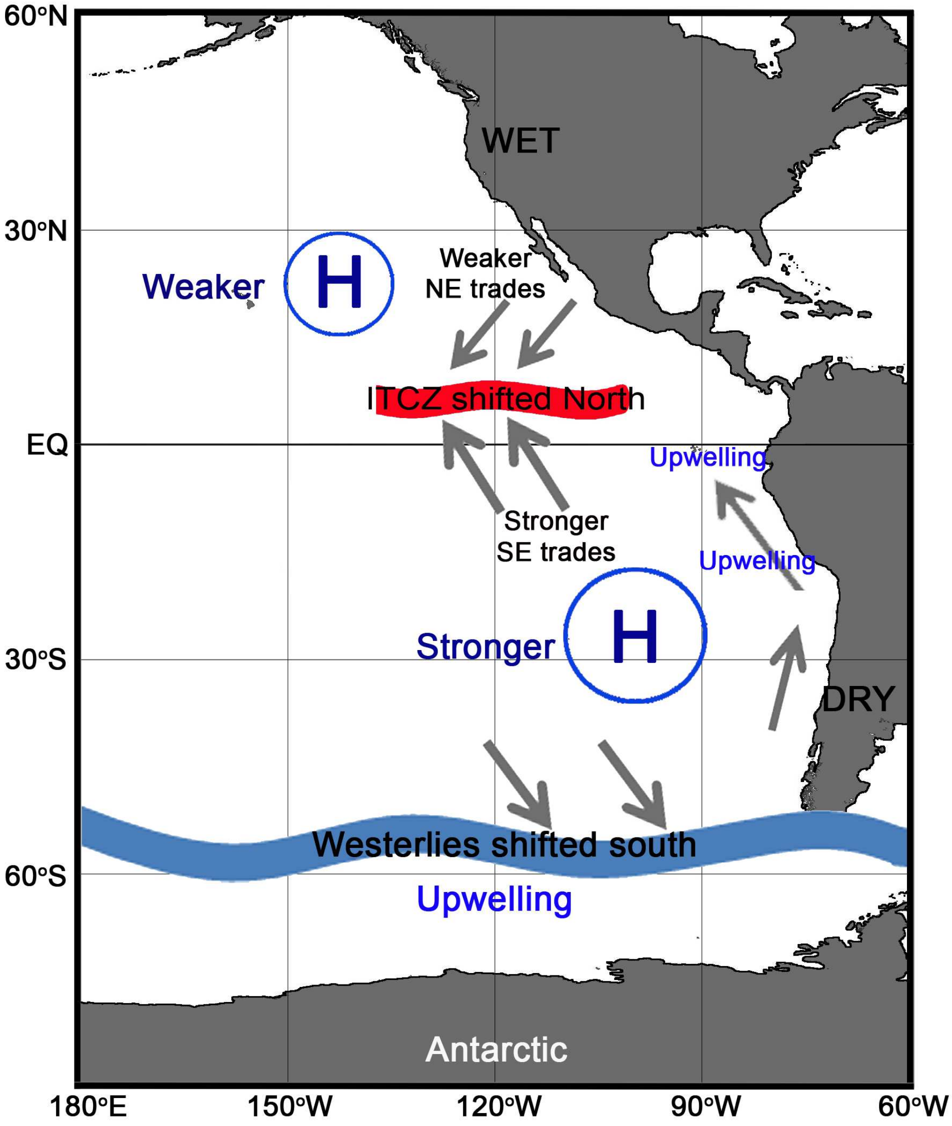

Figure 6. Ocean and atmospheric conditions in the eastern Pacific region during deglaciations. The weaker North Pacific High and the stronger South Pacific High resulted in the northward shift of the ITCZ, the southward shift of the southern westerlies and the intensification of upwelling in the EEP, the Peru margin and the Southern Ocean.

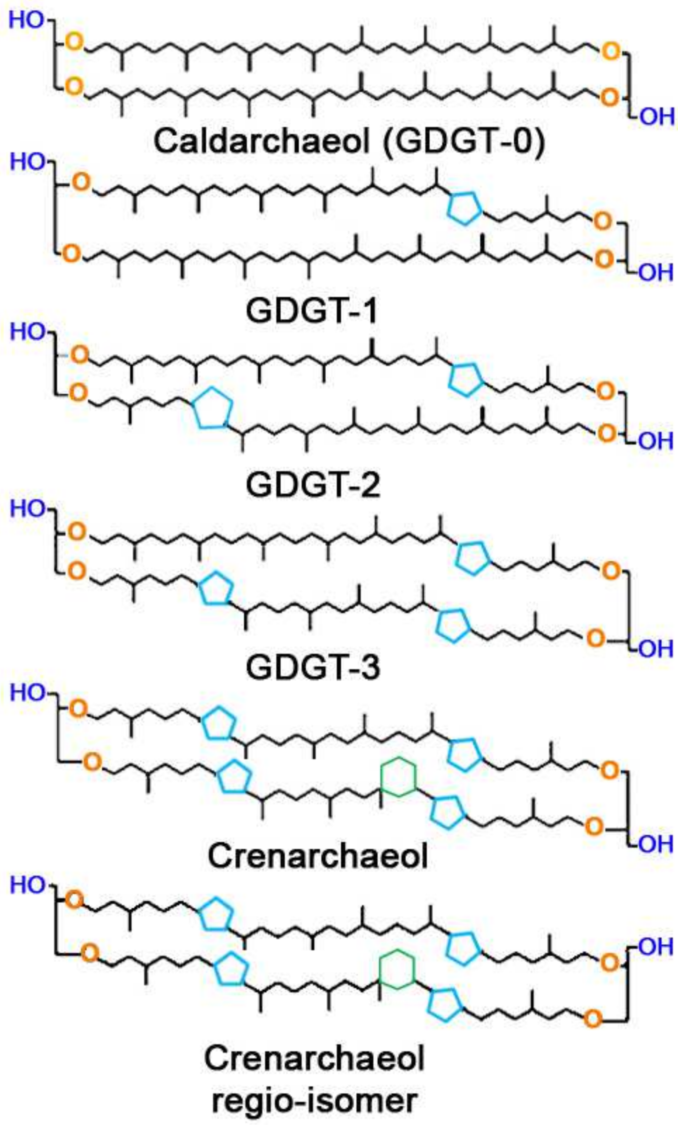

Appendix I. Structure of glycerol dialkyl glycerol tetraethers